J Solid State Electrochem (2012) 16:2899–2906
DOI 10.1007/s10008-012-1722-7

ORIGINAL PAPER

# Cobalt electrodeposition on polycrystalline palladium. Influence of temperature on kinetic parameters

**L. H. Mendoza-Huizar · C. H. Rios-Reyes**

Received: 24 April 2011 / Revised: 6 March 2012 / Accepted: 8 March 2012 / Published online: 25 March 2012


**Abstract** Cobalt electrodeposition on polycrystalline palladium was studied at different temperatures using potentiostatic and voltammetric techniques. Temperature effect on kinetics parameters, diffusion coefficient, and charge transfer coefficient was analyzed. The values of nucleation rate and rate constant of the proton reduction reaction ($k_{PR}$) increased with the temperature increment and the applied overpotential. The number of active nucleation sites was slightly affected with temperature increase. At higher temperatures, the larger $k_{PR}$ values suggested the proton reduction process is favored. The temperature effect on the values of the transfer coefficient was analyzed and a decrease in its value with the temperature increase was observed. From a Conway plot, it was observed that entropy change is the main factor that controls the kinetics of the reaction in this system.

**Keywords** Cobalt · Temperature · Electrodeposition · Palladium · Kinetic

L. H. Mendoza-Huizar · C. H. Rios-Reyes
Area Académica de Quimica,
Universidad Autónoma del Estado de Hidalgo,
Carretera Pachuca-Tulancingo km. 4.5,
42186 Mineral de la Reforma, Hidalgo, Mexico

C. H. Rios-Reyes
Área Académica de Ciencias de la Tierra y Materiales,
Universidad Autónoma del Estado de Hidalgo,
Carretera Pachuca-Tulancingo km. 4.5,
42186 Mineral de la Reforma, Hidalgo, Mexico

L. H. Mendoza-Huizar (✉)
Centro de Investigaciones Químicas,
Universidad Autónoma del Estado de Hidalgo,
Mineral de la Reforma, Hidalgo 42186, Mexico
e-mail: hhuizar@uaeh.edu.mx

## Introduction

Cobalt films deposited on different substrates have been studied because they present perpendicular magnetic anisotropy [1, 2]. This characteristic makes them promising candidates to build new magneto-optical (MO) storage devices [1, 2]. Co deposited on Pd (Co/Pd) and Pt (Co/Pt) shows an increase in the orbital momentum compared with bulk Co [3] which is useful for increasing the capacities of information storage media [4]. Besides, Co/Pd systems allow a better control of the coercivity in comparison with Co/Pt systems, which is important for keeping the stability of the stored information in MO devices [5–7]. Co/Pd systems may be obtained through techniques such as low-energy ion scattering spectroscopy [8], X-ray photoelectron spectroscopy [9], sputtering [10], vapor deposition [11, 12], and more recently electrodeposition [6, 13–19]. Although, the electrodeposition is an economical and simple technique; it requires a good knowledge of the nucleation and growth parameters in order to get cobalt films with reproducible characteristics. Only few studies have considered electrodeposition as an alternative during the synthesis of Co films [6, 13]. This is because the simultaneous cobalt reduction and hydrogen evolution makes difficult the cobalt electrodeposition on palladium. Thus, a better understanding of the deposition will provide a good control of their morphological, magnetic, and electronic properties. Despite the technological importance of cobalt thin films fabrication on palladium, to our knowledge, there is no kinetic information about the cobalt electrodeposition on polycrystalline palladium. Therefore, to gain a deeper insight into this system, in the present paper, we report a kinetic study of the cobalt electrodeposition on polycrystalline palladium by using cyclic voltammetry and chronoamperometry. Finally, we also analyzed temperature effect on kinetic parameters related to electrodeposition process.

## Methodology

Cobalt electrodeposits on palladium were carried out from an aqueous solution containing 0.01 M $CoCl_2$+1 M $NH_4Cl$ at pH 4.5 at 298, 303, 308, and 313 K. We select these temperatures because evaporation problems are negligible in these conditions. Thus, the effect of potential and temperature may be studied without any variation in the solution concentration. All solutions were prepared using analytic grade reagents with ultra pure water (Millipore-Q system) and were deoxygenated by bubbling $N_2$ for 15 min before each experiment. Once the solution was deoxygenated, a nitrogen atmosphere was maintained over the solutions. The working electrode was a palladium tip provided by BAS™ with 0.071 $cm^2$; the exposed surface was polished to a mirror finish with different grades of alumina down to 0.05 μm and ultrasonically cleaned before experiments. A graphite bar with an exposed area greater than the working electrode was used as counter electrode. An Ag/AgCl (Sat KCl) electrode was used as reference electrode with all measured potentials referred to this scale. In all cases, the reference electrode potential was corrected according to the methodology reported in literature [20]. The electrochemical experiments were carried out with a BAS potentiostat connected to a personal computer running the BAS100W software to allow control of experiments and data acquisition. In order to verify the electrochemical behavior of the electrode in the electrodeposition bath, cyclic voltammetry was performed in the 0.400 to −1.100 V potential range at different scan rates. In all experiments, the resistance of the solution was taken into account through the electronic compensation provided by the equipment. The kinetic mechanism of cobalt deposit on Pd was studied under potentiostatic conditions by the analysis of the experimental current density transients obtained with the potential step technique. The perturbation of the potential electrode always started at 0.600 V. The bath temperature was controlled with a Techne Tempette TE-8D temperature controller.

## Results and discussion

### Voltammetric study

Under our experimental conditions, it has been reported the predominant chemical species of cobalt corresponds to the $[Co(H_2O)_6]^{2+}$ complex and the equilibrium potential of the $[Co(H_2O)_6]^{2+}/Co^0$ couple is −0.540 V vs. Ag/AgCl [21]. Thus, the deposition of cobalt that occurs at potentials more positive than the equilibrium potential is defined as occurring at underpotential conditions (upd), while the cobalt deposition that takes place at more negative potentials is called overpotential deposition (opd). In Fig. 1, typical cyclic voltammograms obtained from the system, Pd/0.01 M $CoCl_2$+ 1 M $NH_4Cl$ at 298, 303, 308, and 313 K are shown. In all cases, it is possible to observe the presence of a peak A in the cobalt upd zone. As the electrode potential changes to more negative values, another current density peak B is formed at approximately −0.9 V, in the cobalt opd zone. Note after peak B that there is a change of slope due to the hydrogen evolution on electrodeposited cobalt. During the inverse potential scan, the peaks C, D, and E may be associated with the cobalt dissolution previously deposited during the direct scan [22].

In order to analyze if peak A corresponds to a cobalt upd process, we performed a cyclic voltammetry measurement of the palladium electrode immersed in an aqueous solution only containing the supporting electrolyte (1 M $NH_4Cl$). Figure 2 shows a comparison of the experimental voltammograms obtained at the palladium electrode in both solutions, with and without $Co^{2+}$ ions. From the comparison, clearly peak A is due to the supporting electrolyte and it is not related to a cobalt upd process. The same results were obtained at different temperatures used in this work. Similar electrochemical signals with peak A have been recorded on polycrystalline palladium from acid ammoniacal solutions [23]. In such studies, these signals have been associated with a hydrogen evolution following a multistep reaction which is explained by a Volmer–Heyrovsky–Tafel mechanism [23]. The first step in such process is the formation of adsorbed hydrogen atoms on the surface (the Volmer reaction)

$$H_3O^+ + e^- \rightarrow H^{\bullet}_{ads} + H_2O \quad (1)$$

where $H^{\bullet}_{ads}$ is an adsorbed hydrogen atom at the palladium surface. This is followed by the combination of two adsorbed hydrogen atoms to give molecular hydrogen (the Tafel reaction)

$$H^{\bullet}_{ads} + H^{\bullet}_{ads} \rightarrow H_2 \quad (2)$$

To find out the control that limits the cobalt electrodeposition associated with peak B, the current density value

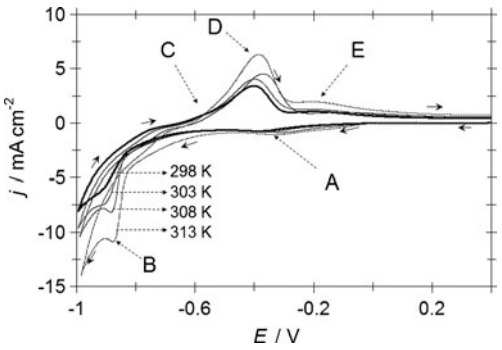


**Fig. 1** Typical cyclic voltammograms plots obtained from the Pd/$10^{-2}$ M $CoCl_2$+1 M $NH_4Cl$ at pH 4.5 at different temperatures as is indicated in the figure. In all cases, the potential rate started at 0.600 V towards the negative direction with a potential scan rate of 50 mV $s^{-1}$

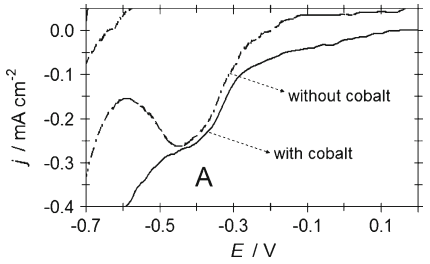


**Fig. 2** A comparison of two cyclic voltammetric curves obtained in the Pd/$x$ M $CoCl_2$+1 M $NH_4Cl$ (pH 4.5) system at two different $CoCl_2$ concentrations, **a** $x$=0 (*broken line*) and **b** $x=10^{-2}$ M (*straight line*). The potential scan started at **a** 0.600 V and **b** 0.400 V towards the negative direction with a scan potential rate of 50 mV $s^{-1}$. *Arrows* potential scan direction. The cathodic current density peak A is also indicated

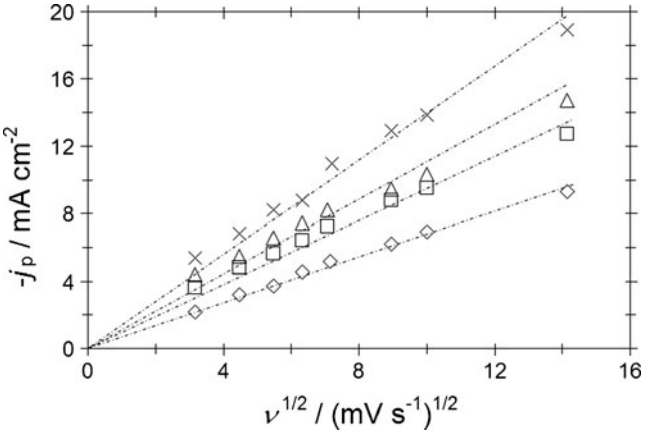


**Fig. 3** Plot of the experimental cathodic peak current density B ($j_p$) as a function of scan rate ($\nu^{1/2}$) for different temperatures. The *broken straight line* corresponds to the linear fit to the experimental data

associated ($j_p$) was plotted as a function of $\nu^{1/2}$ according to Berzins–Delahay equation (Eq. 3) [24]:

$$j_p = \frac{i_p}{S} = 367 n^{3/2} C_0 D^{1/2} \nu^{1/2}, \quad (3)$$

in this equation, $i_p$ is the peak current value in Amperes, $n$ is the number of electrons transferred, $S$ is the area in square centimeter, $C_0$ is the molar concentration in bulk, $D$ is the diffusional coefficient in square centimeter per second, and $\nu$ is the potential scan rate in volt per second. Here, it is important to mention that as soon as metallic cobalt appeared on the surface of the electrode, it served as a reaction site for hydrogen evolution and the current recorded for cobalt electrodeposition is indistinguishable from hydrogen evolution reaction and the current associated to the peak B may be the result of two contributions. In order to verify the influence of the hydrogen evolution in peak B, we carried out a linear voltammetry in the 0.400 to −0.900 V potential range at different scan rates, switch potentials, and temperatures analyzed in present work (not shown). In each case, we performed the dissolution of the deposits in a solution containing only the supporting electrolyte. We compared the cathodic charge with the anodic charge; in all cases, the contribution of hydrogen reduction to the current recorded in the peak B was in average 6 %. Figure 3 shows the plot of the corrected $j_p$ vs. $\nu^{1/2}$ at different temperatures, note a linear relationship which suggests a cobalt ion diffusion control process. It is interesting to note that according to the Berzins–Delahay equation, the current should vanish as the potential scan rate approaches zero. The data shown in Fig. 3 suggest the current intercept is negative at 298 K, while positive at the higher temperatures. Berzins and Delahay have suggested that this partial inconsistency is because Eq. (3) was derived considering an infinite dilution [24]. Besides, they pointed out that in the theoretical treatment the activity of the deposit is equal to unity. Here, it is important to consider that at the initial potential of the voltage sweep, no metal is deposited on the electrode. Thus, the activity of the deposit at the initial potential of the wave is smaller than unity. However, as soon as a low current has flowed through the cell, a sufficiently large number of atoms of metal have been produced to coat the electrode. Once these atoms have been produced, the activity of the deposit can be regarded as equal to unity and the theoretical treatment is valid. Thus, at lower scan rates, the peak potential value is more cathodic than the theoretical value. In contrast, at higher scan rates, the peak potential is shifted toward the theoretical value as the rate of potential is increased [24]. Therefore, we performed a linear fitting of the current peak considering that at higher scan rates the behavior is the predicted by Eq. (3) and we imposed the inception as located in the axes interception. The linear fitting is shown in Fig. 3 as a broken line. In all cases, a linear relationship was found. From the slope's value and Eq. (3), it was possible to calculate the diffusion coefficient value at each temperature. The values calculated were $3.32\ 10^{-6}$, $5.06\ 10^{-6}$, $6.82\ 10^{-6}$, and $9.15\ 10^{-6}$ $cm^2\ s^{-1}$ for 298, 303, 308, and 313 K, respectively. The last results are similar to those reported in literature for cobalt electrodeposition on different substrates [16, 17, 21]. The diffusion coefficients calculated were fitted with the Arrhenius equation (Eq. 4):

$$D = D^0 \exp\left(-\frac{\Delta H_D}{RT}\right), \quad (4)$$

where $D^0$ is the limiting diffusion, $\Delta H_D$ the activation energy of the diffusion process, $R$ the gas constant, and $T$ is the temperature in Kelvin. From the variation of the logarithm of the diffusion coefficient versus $1/T$, the next equation was obtained

$$\log D = 3.64 - \frac{2712}{T}, \quad (5)$$

From the last equation, the value of $\Delta H_D$ was calculated as 22.55 kJ $mol^{-1}$, similar values have been reported for others systems [25].

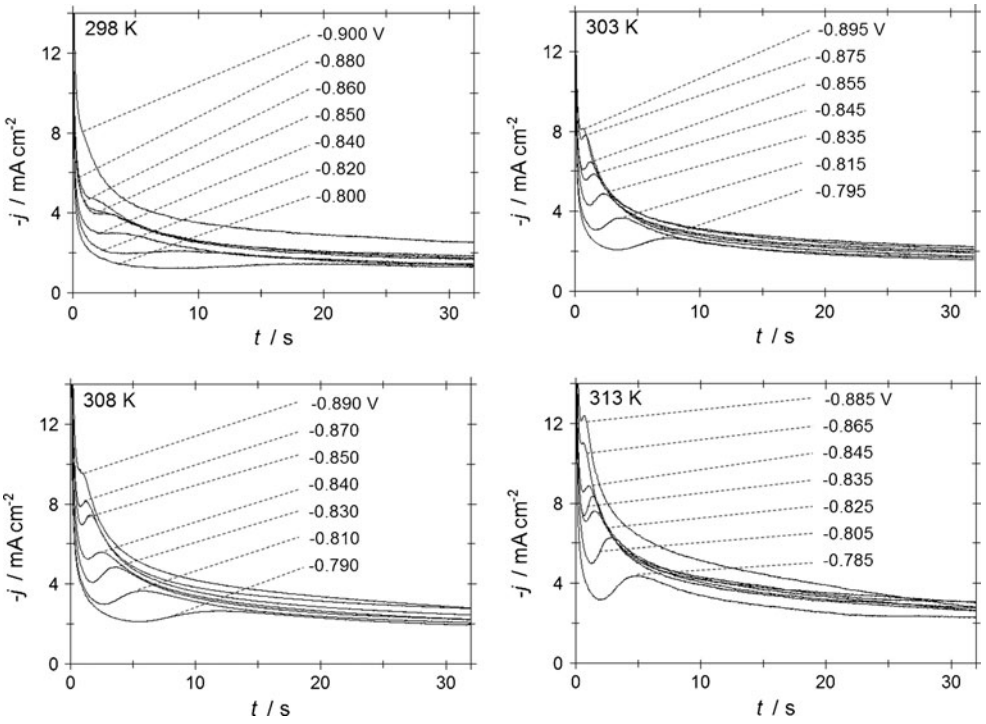


**Fig. 4** Experimental current transients recorded in the Pd/$10^{-2}$ M $CoCl_2$+1 M $NH_4Cl$ (pH 4.5) system at different negative potentials values. In all cases, a starting potential of 0.600 V was applied to the palladium electrode surface

## Chronoamperometric study

It is well known that current transients can provide valuable information about the kinetics of the electrodeposition process. Thus, in this work, we perform a kinetic study employing the chronoamperometric technique to evaluate the kinetic parameters associated with the nucleation and growth of cobalt on palladium. Figure 4a–d shows a set of current density transients recorded at different temperatures by using a step potential technique. These transients were obtained by applying an initial potential at 0.600 V on the Pd surface electrode. At this potential value, the Co deposition still had not begun. After the application of this initial potential, a negative potential step was applied on the surface of the electrode within the potential range [−0.800 to −0.900] V. At shorter times, the current density transients depicted in Fig. 4 show a current decrease which is associated with an adsorption process [26]. Note that after this falling current, in each case, the $j$ vs. $t$ plot passes through a maximum and then approaches the limiting diffusion current to a planar electrode. This behavior has been related to multiple 3D nucleation and growth processes controlled by a mass transfer reaction [27, 28]. The last results and those obtained from the voltammetric study suggest a diffusion-controlled process of the cobalt electrodeposition on palladium.

From diffusional controlled current density transients, it is possible to classify the nucleation as instantaneous or progressive by following the Sharifker's equations [27]. Thus, the experimental transients in a nondimensional form of $j^2/j_m{}^2$ vs. $t/t_m$ are compared with those theoretically

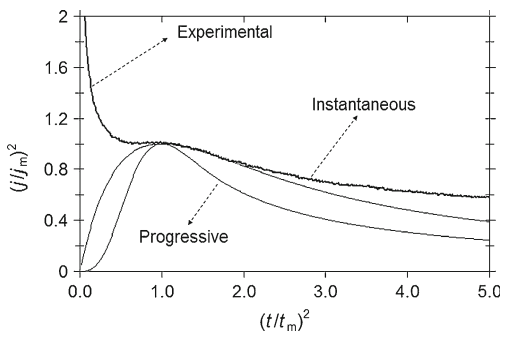


**Fig. 5** Comparison of an experimental transient normalized (through the coordinates of its respective local maximum ($t_m$, $j_m$)), with the theoretical nondimensional curves corresponding to 3D instantaneous nucleation (Eq. (6)) and 3D progressive nucleation (Eq. (7))

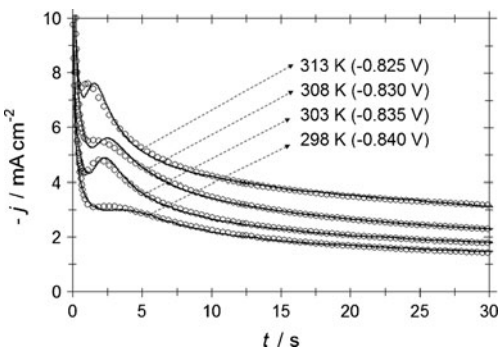


**Fig. 6** Comparison between experimental current density transients (*straight line*) recorded at different temperatures and potentials during the Co electrodeposition on polycrystalline palladium with its theoretical transient (OOO) generated by nonlinear fitting of Eq. (18) to the experimental data

**Table 1** Potential dependence for the nucleation rate parameter ($A$) during Co electrodeposition onto palladium from an aqueous solution containing 0.01 M $CoCl_2$+1 M $NH_4Cl$ at pH 4.5

| $-E$/V | $T$ (298 K) | $-E$/V | $T$ (303 K) | $-E$/V | $T$ (308 K) | $-E$/V | $T$ (313 K) |
|---|---|---|---|---|---|---|---|
| 0.800 | 4.27 | 0.795 | 5.00 | 0.790 | 5.13 | 0.785 | 3.32 |
| 0.820 | 6.40 | 0.815 | 7.60 | 0.810 | 5.97 | 0.805 | 6.00 |
| 0.840 | 6.39 | 0.835 | 7.74 | 0.830 | 7.93 | 0.825 | 7.93 |
| 0.850 | 8.76 | 0.845 | 8.00 | 0.840 | 7.95 | 0.835 | 7.94 |
| 0.860 | 8.80 | 0.855 | 8.70 | 0.850 | 8.71 | 0.845 | 9.23 |
| 0.880 | 9.28 | 0.875 | 10.77 | 0.870 | 10.32 | 0.865 | 10.54 |
| 0.900 | 12.39 | 0.895 | 10.25 | 0.890 | 11.23 | 0.885 | 11.42 |

The values were obtained from best-fit parameters found through the fitting process of the experimental $j$–$t$ plots using Eq. (18)

generated from Eqs. (6) and (7) for the instantaneous and progressive nucleation, respectively.

$$\frac{j^2}{j_m^2} = 1.9254\left(\frac{t}{t_m}\right)^{-1}\left\{1-\exp\left[-1.2564\left(\frac{t}{t_m}\right)\right]\right\}^2, \quad (6)$$

$$\frac{j^2}{j_m^2} = 1.2254\left(\frac{t}{t_m}\right)^{-1}\left\{1-\exp\left[-2.3367\left(\frac{t}{t_m}\right)^2\right]\right\}^2, \quad (7)$$

Figure 5 shows a general comparison of the theoretical dimensionless transients, obtained by Eqs. (6) and (7) with the experimental dimensionless current transients obtained in the present work. It is important to mention that from these plots, it was not possible to classify the nucleation process as instantaneous or progressive. This may be indicative of the presence of other contributions to the overall current during the early stages of the cobalt deposition process apart from the 3D nucleation contribution [17, 29]. Rios-Reyes et al. have suggested that for the cobalt electrodeposition, the additional contribution is due to the proton reduction process [29]. Also, the presence of the shoulder C, see Fig. 1, suggests the existence of a hydrogen rich Co phase [22]. It has been proposed that when the proton reduction occurs simultaneously with the diffusion-limited 3D growth of Co centers, the overall current density is given by [30]:

$$j(t)_{3D} = \left\{P_1^* + P_4(t-u)^{-1/2}\right\} \times\left\{1-\exp\left[(t-u)-\frac{1-\exp(-P_3(t-u))}{P_3}\right]\right\}, \quad (8)$$

$$P_1^* = P_1\left(\frac{2cM}{\pi\rho}\right)^{1/2}, \quad (9)$$

$$P_1 = z_{PR}Fk_{PR}, \quad (10)$$

$$P_2 = N_0\pi kD, \quad (11)$$

$$P_3 = A, \quad (12)$$

$$P_4 = \frac{2FD^{1/2}c}{\pi^{1/2}}, \quad (13)$$

$$k = \left(\frac{8\pi c}{\rho}\right)^{1/2}, \quad (14)$$

**Table 2** Potential dependence for the number of active nucleation sites ($N_0$ $10^{-5}$ per square centimeter) during Co electrodeposition onto palladium from an aqueous solution containing 0.01 M $CoCl_2$+1 M $NH_4Cl$ at pH 4.5

| $-E$/V | $T$ (298 K) | $-E$/V | $T$ (303 K) | $-E$/V | $T$ (308 K) | $-E$/V | $T$ (313 K) |
|---|---|---|---|---|---|---|---|
| 0.800 | 0.063 | 0.795 | 0.152 | 0.790 | 0.207 | 0.785 | 0.321 |
| 0.820 | 0.152 | 0.815 | 0.332 | 0.810 | 0.331 | 0.805 | 0.471 |
| 0.840 | 0.322 | 0.835 | 0.619 | 0.830 | 0.709 | 0.825 | 0.744 |
| 0.850 | 0.651 | 0.845 | 0.684 | 0.840 | 0.739 | 0.835 | 0.821 |
| 0.860 | 0.664 | 0.855 | 0.685 | 0.850 | 0.780 | 0.845 | 1.371 |
| 0.880 | 0.681 | 0.875 | 0.712 | 0.870 | 0.893 | 0.865 | 2.171 |
| 0.900 | 0.691 | 0.895 | 0.724 | 0.890 | 1.396 | 0.885 | 2.770 |

The values were obtained from best-fit parameters found through the fitting process of the experimental $j$–$t$ plots using Eq. (18)

**Table 3** Potential dependence for the rate constant of the proton reduction reaction ($k_{PR}$ $10^5$ mol cm$^{-2}$ s$^{-1}$) during Co electrodeposition from Pd/01 M $CoCl_2$+1 M $NH_4Cl$ system

| $-E$/V | $T$ (298 K) | $-E$/V | $T$ (303 K) | $-E$/V | $T$ (308 K) | $-E$/V | $T$ (313 K) |
|---|---|---|---|---|---|---|---|
| 0.800 | 0.932 | 0.795 | 2.398 | 0.790 | 4.024 | 0.785 | 6.220 |
| 0.820 | 1.251 | 0.815 | 2.533 | 0.810 | 5.099 | 0.805 | 9.973 |
| 0.840 | 1.330 | 0.835 | 3.289 | 0.830 | 5.656 | 0.825 | 10.254 |
| 0.850 | 3.497 | 0.845 | 4.165 | 0.840 | 5.772 | 0.835 | 8.376 |
| 0.860 | 2.833 | 0.855 | 4.437 | 0.850 | 6.860 | 0.845 | 10.451 |
| 0.880 | 3.021 | 0.875 | 5.374 | 0.870 | 8.273 | 0.865 | 9.963 |
| 0.900 | 7.430 | 0.895 | 5.595 | 0.890 | 9.412 | 0.885 | 13.210 |

The values were obtained from best-fit parameters found through the fitting process of the experimental $j$–$t$ plots using Eq. (18)

where $z_{PR}$F is the molar charge transferred during the proton reduction process, $k_{PR}$ is the rate constant of the proton reduction reaction, $N_0$ is the number of active nucleation sites, $A$ is the nucleation rate, $D$ is the diffusion coefficient, $F$ is the Faraday's constant, $u$ is the induction time, and all others parameters have their conventional meanings. Moreover, the peak A in the voltammetric study and the initial falling current recorded in the transients showed in Fig. 4 suggest the existence of an adsorption process, which may be modeled by [31, 32]:

$$j_{ad}(t) = k_1 \exp(-k_2 t) \tag{15}$$

where,

$$k_1 = k_2 q_{ads}, \tag{16}$$

$q_{ads}$ is the total charge for the adsorption process. The potential dependence of $k_2$ is assumed to obey the Butler–Volmer relation [33]. Then the adsorption of metal ions associated with a charge transfer is given by

$$k_2 = k_a^0 \exp\left[-\frac{(1-\beta)\mathrm{nFE}}{RT}\right] \tag{17}$$

$k_a^0$ is an adsorption constant and all others parameters have their conventional meanings.

Thus, we propose the total current of transients depicted in Fig. 4 can be predicted by:

$$j_{total}(t) = j_{3D}(t) + j_{ad}(t) \tag{18}$$

Figure 6 shows a typical comparison of some experimental current density transients with the theoretically generated nonlinear fitting of experimental data to Eq. (18). It can be observed that the model expressed by Eq. (18) adequately accounted for the behavior of the experimental transients. The physical parameters calculated from the fittings are summarized in Tables 1, 2, and 3. It is interesting to observe the nucleation rate increases with the temperature increment and the applied overpotential (see Table 1). A similar behavior for the nucleation rate has been reported for the silver electrodeposition on GCE and the copper electrodeposition on SSE electrode [34, 35]. On the other hand, the $N_0$ values were slightly augmented with the temperature increase and the applied overpotential (see Table 2). Mostany et al. found similar results for the silver electrodeposition from nitrate solutions on glassy carbon electrodes [36].

In all cases, an increase in the $k_{PR}$ values was obtained with the temperature increment and the applied overpotential (see Table 3). This result indicates the proton reduction process is favored and there is a competition by the active

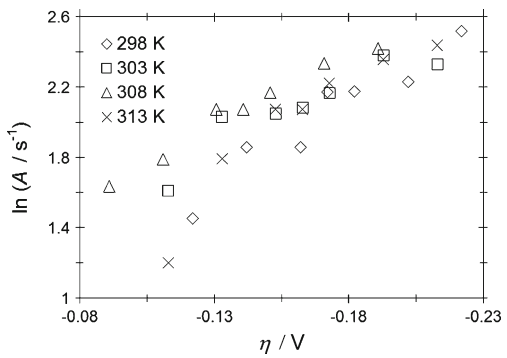


**Fig. 7** In $A$ vs. $\eta$ plot for each temperature is used to calculate the critical nuclei's size according to Eq. (19)

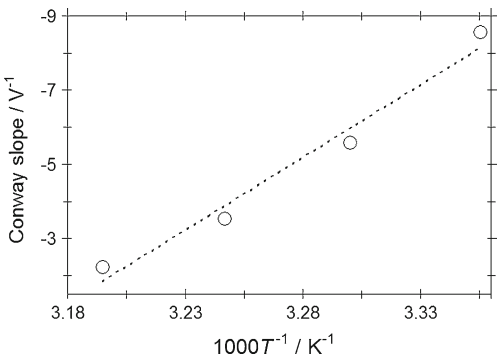


**Fig. 8** Conway's plot of the reciprocal Tafel's slope versus the reciprocal absolute temperature according to Eq. (22)

sites on the surface by $H^+$ ions with the $Co^{2+}$ cations as the temperature increases.

Through the physical constants reported in Table 1, it is possible to estimate the critical size of the cobalt nucleus in the framework of the atomistic theory of electrolytic nucleation by using the following equation [37]:

$$n_c = \left(\frac{k_B T}{z e_0}\right) \frac{d \ln A}{d\eta} \tag{19}$$

The plots $\ln A$ vs. $\eta$ showed a linear tendency (see Fig. 7). The values of $d(\ln A)/d(\eta)$ were 9.64, 6.78, 8.09, and 11.45 for 298, 303, 308, and 313 K, respectively. The critical cluster's size calculated was $n_c$=0 for all temperatures. This value means that each active site is a critical nucleus.

$k_{PR}$ values reported in Table 3 can be modeled following a Butler–Volmer type relationship [21] by using the next equation:

$$k_{PR} = k_{PR}^0 \exp\left[-\frac{\alpha_{PR} z F E}{R T}\right] \tag{20}$$

From the slope of the $\ln k_{PR}$ versus $E$ plot, it is possible to estimate the $\alpha_{PR}$ value. The results calculated were 0.51, 0.33, 0.22, and 0.14 for 298, 303, 308, and 313 K, respectively. It is interesting to note that the transfer coefficient for the hydrogen evolution reaction in this system decreases with the temperature increase. In general, the transfer coefficient $\alpha$ varies with the absolute temperature following the linear relationship suggested by Conway [38–41]:

$$\alpha = \alpha_H + \alpha_s T \tag{21}$$

where $\alpha_H$ and $\alpha_S$ are the enthalpic and entropic components, respectively. According to this equation, the Tafel's slope can be represented as:

$$b = -\frac{2.3RT}{(\alpha_H + \alpha_s T)F} \tag{22}$$

where $\alpha_H$ and $\alpha_S$ can be evaluated by plotting the reciprocal of Tafel's slope versus the reciprocal of $T$, i.e., as a Conway plot. Figure 8 shows this plot which follows a linear tendency. From the slope and the intercept of this line, $\alpha_H$ and $\alpha_S$ were calculated as $\alpha_H$=−7.78 $10^{-3}$ and $\alpha_S$=2.45 $10^{-2}$ $K^{-1}$. Note that the entropy transfer coefficient is the controlling factor for the catalytic activity of the electrochemical reaction suggesting that activation entropy plays one of the most important roles in this process. Thus, entropy change is the principal factor which is controlling the kinetics of the reaction at a given electrode potential.

## Conclusions

In the present work, it was found that the values of the diffusion coefficients were dependent on temperature and their tendency was predicted by the Arrhenius equation. The current density transients were well described through a kinetic mechanism that involves three different contributions: (a) a Langmuir type adsorption process, (b) 3D nucleation limited by a mass transfer reaction, and (c) a proton reduction process. It was found that as the temperature and the overpotential applied were increased, $A$ and $k_{PR}$ were increased. On the other hand, $N_0$ was slightly affected with temperature increase. By using a Conway plot, it was found that the activation entropy played one of the most important roles in cathodic electrochemical process.

**Acknowledgments** CHRR is grateful for a postdoctoral fellowship from CONACYT. LHMH and CHRR thank financial supports from the Universidad Autónoma del Estado de Hidalgo. We acknowledge Professor M. Rivera for fruitful comments.

## References

1. Bakonyi I, Peter L (2010) Prog Mater Sci 55:107–245
2. Oha SJ, Kima W, Kima W, Choia BH, Kima JY, Koha H, Kima HJ, Park JH (2001) Appl Surf Sci 169:127–133
3. Wu Y, Stohr J, Hermsmeier B, Samant MG, Weller D (1992) Phys Rev Lett 69:2307–2310
4. Metoki N, Donner W, Zabel H (1994) Phys Rev B 49:17351–17359
5. Bell BW, Campbell DK (1997) Handbook of magneto-optical data recording: materials, subsystems, techniques. In: McDaniel TW, Victora RH (eds). Noyes Publications: New Jersey
6. Baricuatro JHL (2006) Electrodeposition of ultrathin Pd, Co and Bi films on well-defined noble-metal electrodes: studies by ultrahigh vacuum-electrochemistry (Uhv-Ec). In: Texas A&M University (ed). ProQuest Information and Learning Company, Texas
7. Wu Y, Stohr J, Hermsmeimer BD, Samant MG, Weller D (1992) Phys Rev Lett 69:2307–2310
8. Atrei A, Rovida G, Torrini M, Bardi U, Gleeson M, Barnes CJ (1997) Surf Sci 372:91–105
9. Bardi U (1991) Appl Surf Sci 51:89–93
10. Haan P, Meng Q, Katayama T, Lodder JC (1992) J Magn Magn Mater 113:29–35
11. Broeder FJA, Donkersloot HC, Draaisma HJG, Jonge WJM (1987) J Appl Phys 61:4317–4319
12. Boukari S, Beaurepaire E, Scheurer F, Carriere B, Deville JP (1998) Thin Solid Films 318:177–179
13. Takata FM, Sumodjo PTA (2007) Electrochim Acta 52:6089–6096
14. Georgescu V, Mazur V, Cheloglu O (1996) J Magn Magn Mater 156:27–28
15. Jyoko Y, Kashiwabara S, Hayashi Y (1996) J Magn Magn Mater 156:35–37
16. Georgescu V, Mazur V, Pushcashu B (2000) Mater Sci Eng B 68:131–137
17. Mendoza-Huizar LH, Robles J, Palomar-Pardavé M (2002) J Electroanal Chem 521:95–106
18. Mendoza-Huizar LH, Robles J, Palomar-Pardavé M (2003) J Electroanal Chem 545:39–45
19. Mendoza-Huizar LH, Rios-Reyes CH (2011) J Solid State Electrochem 15:737–745
20. Ives DJG, Janz GJ (1961) Reference electrodes theory and practice. Academic, New York
21. Palomar-Pardave ME, Gonzalez I, Soto AB, Arce EM (1998) J Electroanal Chem 443:125–136
22. Bertazzoli R, Sousa MFB (1997) J Braz Chem Soc 8:357–362

23. Bartlett PN, Gollas B, Guerin S, Marwan J (2002) Phys Chem Chem Phys 4:3835–3842
24. Berzins T, Delahay P (1953) J Am Chem Soc 75:555–559
25. Matsumiya M, Terazono M, Tokuraku K (2006) Electrochim Acta 51:1178–1183
26. Holzle MH, Retter U, Kolb DM (1994) J Electroanal Chem 371:101–109
27. Scharifker BR, Hills G (1983) Electrochim Acta 28:879–889
28. Scharifker BR, Mostany J (1984) J Electroanal Chem 177:13–23
29. Rios-Reyes CH, Granados-Neri M, Mendoza-Huizar LH (2009) Quim Nova 32:2382–2386
30. Palomar-Pardavé ME, Scharifker BR, Arce EM, Romero-Romo M (2005) Electrochim Acta 50:4736–4745
31. Varela FE, Grassa LM, Vilche JR (1992) Electrochim Acta 37:1119–1127
32. Barradas RG, Bosco E (1985) J Electroanal Chem 193:23–26
33. Noel M, Vasu K (1990) Cyclic voltammetry and the frontiers of electrochemistry. Aspect, London
34. Ramírez C, Arce EM, Romero-Romo M, Palomar-Pardave ME (2004) Solid State Ionics 169:81–85
35. Vazquez-Arenas J, Cruz R, Mendoza-Huizar LH (2006) Electrochim Acta 52:892–903
36. Mostany J, Scharifker BR, Saavedra K, Borrás C (2008) Russ J Electrochem 44(6):652–658
37. Milchev A (1991) J Contemp Phys 32:321–332
38. Conway BE, MacKinnon DJ, Tilak BV (1970) Trans Faraday Soc 66:1203–1226
39. Conway BE, Wilkinson DF (1986) J Electroanal Chem Interfacial 214:633–653
40. Conway BE (1985) The temperature and potential dependence of electrochemical reaction rates, and the real form of the Tafel equation. In: Conway BE, White RE, Bockris JOM (eds) Modern aspects of electrochemistry no. 16. Plenum, New York
41. Conway BE, Tessier DF, Wilkinson DP (1986) J Electroanal Chem Interfacial Electrochem 199:249–269